2017 International Conference on Medicine Sciences and Bioengineering (ICMSB 2017)
ISBN: 978-1-60595-508-7

Computational Hemodynamics of Aneurismal Model in the Circle of Willis Virtually Treated with Closed Cell and Open Cell Stent

Wen-Yu FU[1] and Ai-Ke QIAO[2]

[1]College of Mechanical and Electrical Engineering, Beijing Union University, China

[2]College of Life Science and Bioengineering, Beijing University of Technology, China

Keywords: Aneurysm, Circle of Willis, Hemodynamics, Computational fluid dynamics.

Abstract. To investigate the difference of the hemodynamics of aneurismal model in the circle of Willis virtually treated with closed cell and open cell stent, two kinds of stents were constructed. One is Enterprise stent (Closed-cell), and the other is Neuroform stent (open-cell). Five treatment strategies based on the combination of two kinds of stents were used. The computational fluid dynamics of these five different treatment strategies was calculated and the corresponding hemodynamic characteristics of aneurismal model were analyzed. In particular, the effects of different structural stents and their combinations on the blood flow characteristics (streamline, wall shear stress) of the aneurysm cavity were discussed.

Model Construction

Aneurismal Model in the Circle of Willis

In recent years, endovascular stent intervention has become more popular. It is a minimally invasive form of therapy and requires much less money and recovery time after an operation [1, 2]. To investigate the difference of the hemodynamics of aneurismal model in the circle of Willis virtually treated with closed cell and open cell stent, aneurismal model in the circle of Willis should be constructed firstly. Based on the DICOM images obtained from helical scanning, the medical images were processed by three-dimensional segmentation, and the patient-specific aneurismal model in the circle of Willis was established. The aneurysm located in the anterior communicating artery (AComA). The vasculature includes the following vessels: A1 and A2 segments of the left and right anterior communicating arteries (ACA), middle cerebral artery (MCA), and internal carotid artery (ICA). The final aneurysm model was exported in STL format (as shown in Fig.1). To improve the quality of the surface mesh, the surface model was optimized using the methods of edge collapses and diagonal swaps [3].

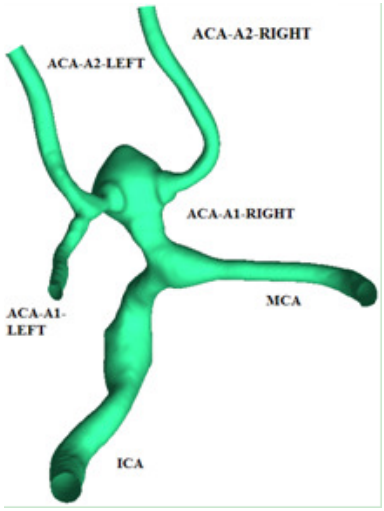

Figure 1. Aneurismal model.

Stent Model

Two different kind of stents, Neuroform-open-cell stent (N-OCS) and Enterprise-closed-cell stent (E-CCS) were constructed. The method of inserting the stent into an aneurismal model included four steps. First, the centerline of aneurismal model was determined. Second, the stent was deformed according to this centerline. Thirdly, both the aneurismal model and the deformed stent model were imported into reverse engineering software of Geomagic (Geomagic Inc, Research Triangle Park, NC). The location of the deformed stent was adjusted repeatedly until an optimal fit was obtained. Fourthly, a boolean operation of subtraction between the aneurysm and the stent geometries was done. In this way, a merged model representing both the assembled vessel and the stent was obtained. Model files were exported in STL format. Using the same method, five assembled models of vessel (CASE1-CASE5, CASE0 is the model without stent) with stent were obtained, as shown in Fig.2.

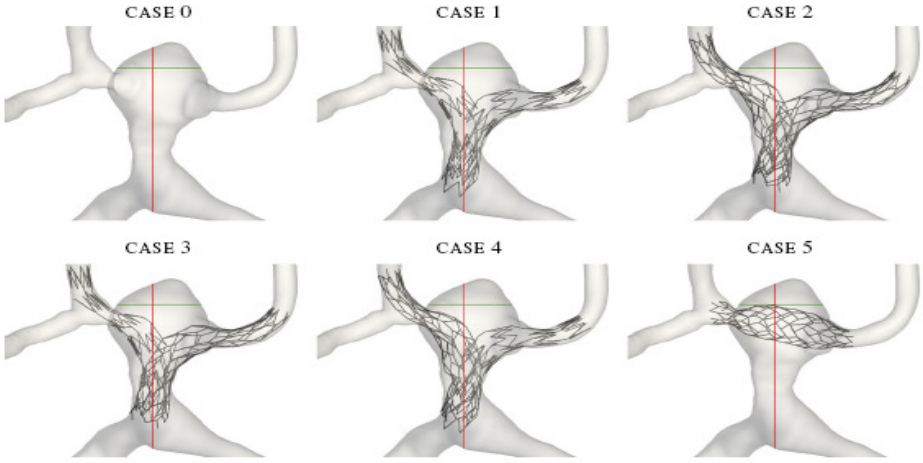

Figure 2. Assembly model of vessel and stent.

The treatment strategies are:

1) N-OCS in A2-left and A2-right; 2) E-CCS in A2-left and A2-right; 3) N-OCS in A2-left and CCS in A2-right; 4) E-CCS in A2-left and OCS in A2-right; 5) N-CCS in ACA-A1

Four treatments (CASE1-CASE4) involve combinations of E-CCSs and N-OCSs deployed in the ACA-A1 and ACA-A2, whereas the 5th treatment (CASE5) is achieved by using a single CCS deployed in the ACA-A1.

Meshing

The model files of STL format were imported into ANSYS ICEM CFD (ANSYS Inc, Canonsburg, PA) and volume meshing was performed. For the purpose of comparison, a numerical simulation of a vessel model without stent was also carried out. Volume meshes of the vessel model without stent were generated using unstructural tetrahedron and prism types. Progressively finer prism meshes were generated near boundary surfaces based on tetrahedral meshes. For models with stents, prism meshes cannot be generated at the boundary layer because of the existence of the stents. Therefore, only tetrahedral meshes were generated for the five models with stents. The size of the resulting grids was reported in Table 1.

Table 1. Number of volume mesh elements corresponding to anatomical unstented (U) and stented (CASE1, CASE2, CASE3, CASE4, CASE5) models.

Model	U	CASE1	CASE 2	CASE 3	CASE 4	CASE 5
Number of meshes	200490	7076801	7298044	7344884	7167882	4502892

Calculation Method

ANSYS CFX 12.0 (ANSYS Inc, Canonsburg, PA) was used to carry out computational fluid dynamics calculation. The average value of Reynolds number based on the entrance flow velocity and the artery diameter is 134, so the flow was assumed to be Newtonian and laminar. Vascular wall was assumed to be rigid [4]. The mass flow rates in the inlets and the outlets are shown in Table 2. Blood flow is controlled by the three-dimensional incompressible Navier-Stokes equations. The viscosity and density of blood are 0.00645Pa•s and 1054kg/m^3 respectively. The no-slip condition was applied to the wall of the vascular and stent. The inlets and outlets of the vascular model are shown in Fig.3. Steady-state flow simulations in this work were carried out to keep CPU times reasonable. The residual convergence criteria of mass and momentum were set to 10^{-6}.

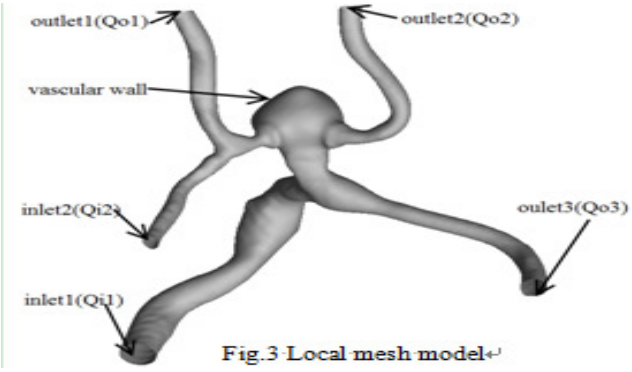

Figure 3. Local mesh model.

Table 2. The mass flow rates in the inlets and outlets.

$Q_{I1}X10^{-4}kg/s$	$Q_{I2}X10^{-4}kg/s$	$Q_{o1}X10^{-4}kg/s$	$Q_{o2}X10^{-4}kg/s$	$Q_{o3}X10^{-4}kg/s$
14.135	4.001	-5.201	-5.73	-7.201

Results

Fig.4 shows the streamlines in aneurismal cavity. The pictures sequence in Fig.4 is the same as in Fig.2. Fig.6 shows that blood flow from the left anterior communicating artery A1 segment enters the left anterior communicating artery A2 segment after implantation of the stent. The vortex flow decreases considerably in model "CASE1" and model "CASE4". The distributions of wall shear stress (wss) on aneurismal wall are shown in Fig.5. For the vascular model without stent, there are regions on aneurismal dome and aneurismal neck where the value of wss is relatively large. Region where the value of wss is relatively large on aneurismal dome disappeared after the implantation of the stent; the aneurysm wall WSS value of the larger part disappeared; after implantation of the tumor the values of wss are reduced on aneurismal neck after the implantation of the stent.

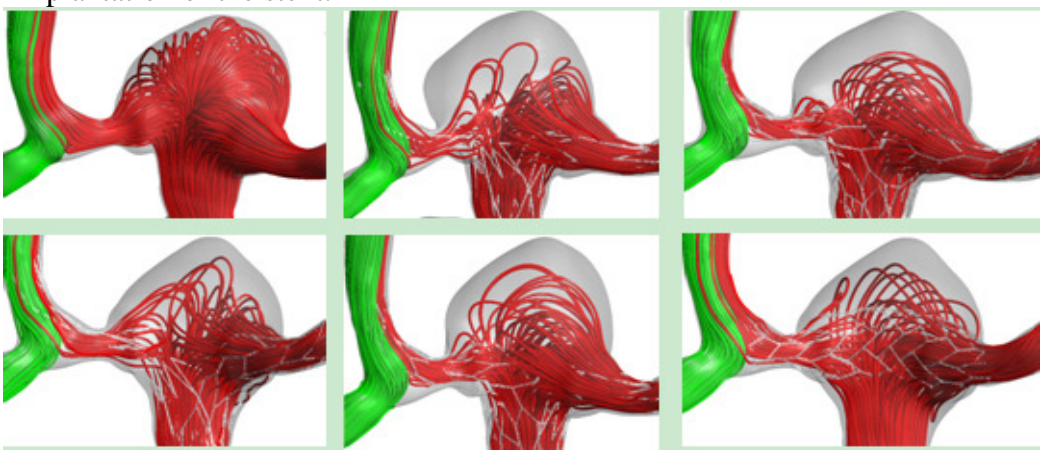

Figure 4. Streamlines in aneurismal cavity.

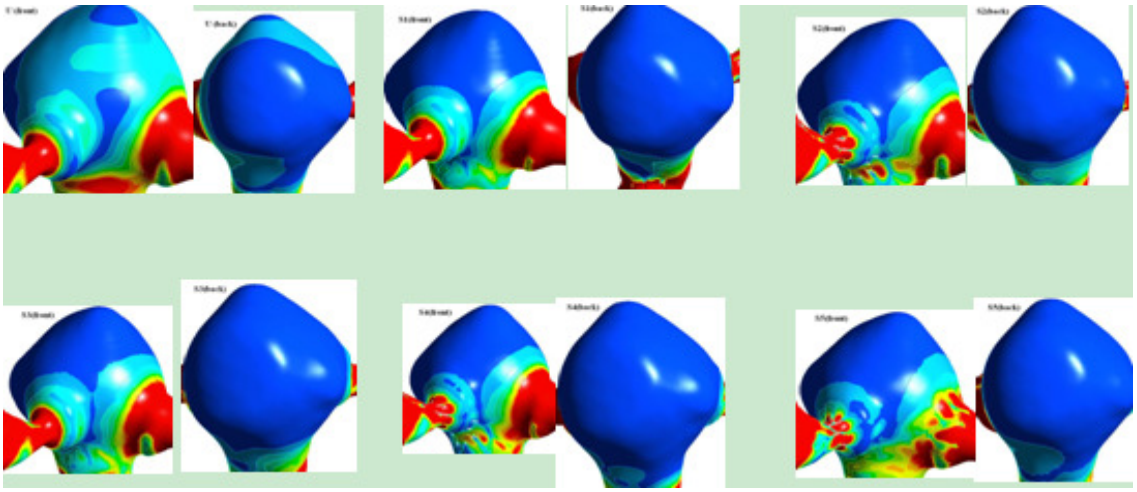

Figure 5. Wall shear stress contour.

Conclusions

Steady flow analyses were performed on the established vascular models. In general, all the blood flow of the left anterior communicating artery A1 enters the left anterior communicating artery A2 segment. Streamlines in blood flow field and the distributions of wss were obtained. In the view of flow reduction in aneurismal cavity, there is no evident difference for the five different strategies of stent deployment. Only one stent was used in CASE5, it has certain advantages (less cost and simple manual operation of deployment stent).

Acknowledgement

This work was supported by the General Program of Science and Technology Development Project of the Beijing Municipal Education Commission of China (KM201711417011)

References

[1] M. Kim, D.B. Taulbee, M. Tremmel, H. Meng, Comparison of two stents in modifying cerebral aneurysm hemodynamics, Annals of Biomedical Engineering, 36(2008), 726-741.

[2] S. Appanaboyina, F. Mut, R. Lohner, C.M. Putman, J.R. Cebral, Computational fluid dynamics of stented intracranial aneurysms using adaptive embedded unstructured grids, International Journal for Numerical Methods in Fluids, 57(2007), 475-493.

[3] J.R. Cebral, R. Löhner, From medical images to anatomically accurate finite element grids, International Journal for Numerical Methods in Engineering, 51(2001), 985-1008.

[4] J.R. Cebral, M.A. Castro, S. Appanaboyina, C.M. Putman, R.D. Millan, A.F. Frangi, Efficient pipeline for image-based patient-specific analysis of cerebral aneurysm haemodynamics: technique and sensitivity, IEEE Transactions on Medical Imaging, 24(2005), 457-467.